Excited-State Reaction Dynamics of Chlorine Dioxide in Water from Absolute Resonance Raman Intensities

Catherine E. Foster and Philip J. Reid*

Department of Chemistry, Box 351700, University of Washington, Seattle, Washington 98195

Received: February 4, 1998; In Final Form: March 10, 1998

Resonance Raman spectra of aqueous chlorine dioxide (OClO) are measured for several excitation wavelengths spanning the photochemically relevant $^2B_1-{}^2A_2$ optical transition. A mode-specific description of the optically prepared, $^2A_2$ potential energy surface is derived by simultaneous analysis of the absolute resonance Raman and absorption cross sections. The resonance Raman spectra are dominated by transitions involving the symmetric stretch and bend coordinates demonstrating that excited-state structural evolution occurs predominately along these degrees of freedom. Scattering intensity is not observed for transitions involving the asymmetric stretch, demonstrating that excited-state structural evolution along this coordinate is modest. The limited evolution along the asymmetric stretch coordinate results in the preservation of C_{2v} symmetry on the $^2A_2$ surface. It is proposed that this preservation of symmetry is responsible for the increase in Cl photoproduct quantum yield in solution relative to the gas phase. Analysis of the absolute scattering cross sections also demonstrates that the homogeneous line width for the $^2B_1-{}^2A_2$ optical transition in water is essentially identical to that in cyclohexane; however, the extent of inhomogeneous broadening increases dramatically in aqueous solution. Comparison of the spectroscopic properties of OClO to the properties of isoelectronic O_3^- is made to elucidate the origin of the solvent response to OClO photoexcitation. It is suggested that solvent−solute dipole−dipole coupling and intermolecular hydrogen bonding represent the largest components of the solvent coordinate.

Introduction

The photochemistry of chlorine dioxide (OClO) is of current interest in atmospheric chemistry due to the participation of this compound in the reactive chlorine reservoir as well as its potential role in stratospheric ozone layer depletion.[1−5] An outline of the photochemical processes available to OClO following photoexcitation is presented in Scheme 1. As the scheme illustrates, photoexcitation of OClO results in the formation of either ClO and O or Cl and O_2.[1,6−49] The Cl and O_2 products may be preceded by the formation of the peroxy isomer of chlorine dioxide, ClOO, produced by the photoisomerization of OClO.[1,26,27,30,32] ClOO has been observed in low-temperature matrixes; however, its presence in the gas or solution phase has yet to be firmly established.[41−43,45,46] The intriguing aspect of this chemistry is that the partitioning between photochemical pathways is dependent on phase. For example, the quantum yield for Cl formation (Φ_{Cl}) in the gas phase is ∼0.04 but is reported to be near unity in low-temperature matrices and on surfaces.[9−11,14−16,40,41,44−46] The chemistry in solution is intermediate between these two limits with $\Phi_{Cl} = 0.1-0.2$ in water and methanol.[26−28,30,32−34] In addition, the mechanism of Cl formation in solution is sensitive to solvent polarity with the Cl + $O_2(^1\Delta_g)$ and Cl + $O_2(^3\Sigma_g^-)$ channels dominating in nonpolar and polar solvents, respectively.[29]

Recent solution-phase studies of OClO have attempted to identify the solvent−solute interactions that influence photoproduct formation. Ultrafast transient absorption spectroscopy has been used to monitor the kinetics of ground-state photoproduct formation.[26,33,34] These studies have provided information on the processes that occur following internal conversion to the ground state (geminate recombination, vibrational relaxation, etc.). We have employed resonance Raman intensity analysis (RRIA) in an attempt to understand how the presence of solvent can influence the excited-state reaction dynamics.[35,36] Using this technique, a mode-specific description of the excited-state potential energy surface can be developed, thereby revealing the reaction dynamics that occur immediately following photoexcitation.[50−52] By performing RRIA on OClO dissolved in a variety of solvents, environmental dependence of the excited-state reaction dynamics can be quantitatively explored. We performed our first studies in cyclohexane where it was anticipated that the weak intermolecular interactions characteristic of this solvent would allow for direct comparison to the dynamics that occur in the gas phase. In particular, analysis of the high-resolution electronic absorption spectrum of gas-phase OClO has demonstrated that evolution along the asymmetric stretch coordinate is an important component of the excited-state structural relaxation.[1,6−8] It was expected that similar dynamics would be observed in cyclohexane; however, we found that the evolution along the asymmetric stretch coordinate is restricted in this solvent.[36] We proposed that dipole−induced dipole interactions between OClO and the surrounding solvent were responsible for modification of the optically prepared excited-state surface along the asymmetric

SCHEME 1

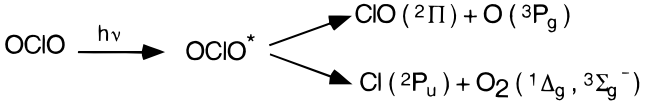

* To whom correspondence should be addressed.

S1089-5639(98)01002-0 CCC: $15.00
Published on Web 04/28/1998

stretch coordinate. The observation that the presence of solvent can influence the excited-state reaction dynamics raises several new questions concerning the condensed-phase reactivity of OClO. What other types of solvent−solute interactions can affect the excited-state dynamics? How do these interactions contribute to the phase- and solvent-dependent photochemical reactivity? Finally, what role does solvent-mediated reactivity play in altering the environmental impact of OClO?

In this paper, we report the analysis of the absolute resonance Raman intensities of OClO dissolved in water. This solvent was chosen for a variety of reasons. First, the dominant solvent−solute interactions between OClO and water are expected to be dipole−dipole coupling and intermolecular hydrogen bonding. These two interactions are expected to be stronger than the dipole−induced dipole coupling operative in cyclohexane; therefore, water provides the opportunity to evaluate the influence of strong, solvent−solute interactions on the excited-state reactivity of OClO. Second, the photochemistry of OClO in aqueous environments is of direct relevance to the environmental impact of this compound. RRIA is capable of providing new insight into the excited-state reaction dynamics of OClO in this environmentally important solvent. Third, recent studies of OClO reactivity in water have involved the application of time-resolved optical spectroscopies with interpretation of these studies dependent on the availability of an accurate description of the optically active $^2A_2$ potential energy surface. RRIA provides an elegant method by which to develop this description.

The RRIA of aqueous OClO presented here provides a detailed description of the excited-state reaction dynamics. The Raman intensities demonstrate that following photoexcitation the excited-state relaxation dynamics are dominated by evolution along the symmetric stretch and bend coordinates. The absence of intensity for transitions involving the asymmetric stretch demonstrates that excited-state evolution along this coordinate is restricted in comparison to the dynamics that occur in the gas phase. The absence of substantial evolution along the asymmetric stretch results in the preservation of C_{2v} symmetry on the $^2A_2$ surface. This observation in combination with recent ab initio theoretical work suggests that the preservation of C_{2v} symmetry is responsible for the increase in Φ_{Cl} in water relative to the gas phase.[47−49] The homogeneous line width for the $^2B_1-{}^2A_2$ transition is found to be 85 ± 15 cm^{-1}. This value is essentially identical to the homogeneous line width determined for OClO dissolved in cyclohexane, suggesting that the energetics and couplings between the excited potential energy surfaces of OClO are not substantially modified by changes in solvent polarity. Finally, a discussion concerning which solvent−solute interactions are operative for aqueous OClO is presented. In particular, comparison is made to recent spectroscopic studies of O_3^-, a species that is isoelectronic with OClO. The large reduction in line width observed for the symmetric stretch fundamental transition of O_3^- in D_2O relative to H_2O is not observed for OClO, demonstrating that the absence of charge results in weaker coupling to the solvent coordinate. Given this observation, it is suggested that for aqueous OClO dipole−dipole coupling and potentially intermolecular hydrogen bonding are the largest components of the solvent coordinate.

Experimental Section

Materials. The absolute Raman intensities of chlorine dioxide (OClO) dissolved in water were measured at 282.4, 319.9, 355, 368.9, 435.7, and 532 nm, using the direct or hydrogen shifted second and third harmonic output of a Nd:YAG laser (Spectra-Physics GCL-170, 30 Hz). The synthesis of gaseous OClO was performed as previously described.[36,53] Solutions of OClO in water were prepared by bubbling gaseous OClO through an aqueous solution of 1 M KNO_3. Adjustment of the OClO concentration was performed by diluting the concentrated aqueous OClO solution with additional amounts of aqueous 1 M KNO_3 to produce the samples employed here. Quantitative addition of KNO_3 was performed such that the NO_3^- transition at 1049 cm^{-1} could be used as an internal standard for determining absolute scattering cross sections (see below).[54,55]

Resonance Raman Spectra. Resonance Raman spectra were obtained by flowing the aqueous OClO sample through a wire guided jet (282.4, 319.9, 355, and 368.9 nm) or square walled glass capillary (355, 368.9, 436, and 532 nm). The sample was delivered at a rate sufficient to replenish the illuminated volume between excitation events. The 135° backscattering geometry was employed in all experiments. The scattered light was collected using standard, UV-quality refractive optics and delivered to a 0.5 or 0.75 m single-stage spectrograph (Acton Research Corp.) equipped with either a classically ruled 1200 grooves/mm or a holographic 2400 grooves/mm grating and a polarization scrambler placed at the spectrograph entrance. Raman scattering was detected with a liquid N_2 cooled 1100 × 330 pixel back-illuminated CCD detector (Princeton Instruments). The intensity of OClO scattering was found to be linear with pump power up to 25 μJ/pulse at 368.9 nm; therefore, <25 μJ pulse energy was used at this wavelength and adjusted at other wavelengths with reference to the absorption cross section of OClO to maintain a homogeneous extent of photoalteration at all excitation points. The OClO concentration was determined by measurement of the absorption spectrum of the sample before and after a given experiment. The overall change in concentration was typically 20% for the open jet and 10% for the glass capillary. The decrease in concentration was dominated by evaporative loss of OClO, and the uncertainty in concentration represents the largest contribution to the error in these measurements. For the temperatures at which the experiments were performed (5 °C), the vapor pressure of OClO is appreciable; therefore, gaseous OClO could also contribute to the observed scattering when the open jet is employed. However, the cross sections determined using both the open jet and closed capillary at 355 nm were identical within experimental error, demonstrating that the scattering contribution from gaseous OClO is negligible. Resonance Raman spectra were corrected for the spectral sensitivity of the instrument using either a calibrated quartz−tungsten−halogen (Oriel) or D_2 emission (Hellma) lamp. Data were also corrected for self-absorption as described previously.[36] Due to the small absorption cross section of OClO, this correction was found to be modest (≤2%).

Depolarization Ratios. In addition to the scattering intensities, the resonance Raman depolarization ratios were measured at each excitation wavelength. The depolarization ratio is defined as the intensity scattered with polarization perpendicular to the incident radiation divided by the scattered intensity with parallel polarization.[56−59] This ratio is needed for calculation of the absolute resonance Raman cross sections in order to correct for the angular dependence of the scattered intensity (see below). The polarization of the incident radiation was defined by passing the excitation beam through six quartz microscope slides oriented at Brewster's angle resulting in a contrast ratio of >1000:1. The polarization of the scattered light was defined using a large-aperture calcite polarizer placed before the polarization scrambler in front of the spectrograph entrance.

TABLE 1: Absolute Raman Cross Sections for Chlorine Dioxide in Water

excitation energy ($\times 10^{-3}$ cm^{-1})	ν_1 ($\times 10^{10}$ Å^2)[a]	$2\nu_1$ ($\times 10^{10}$ Å^2)	ν_2 ($\times 10^{10}$ Å^2)	$2\nu_2$ ($\times 10^{10}$ Å^2)	$2\nu_3$ ($\times 10^{10}$ Å^2)	$\rho(\nu_1)$[b]
18.8	0.06 ± 0.02[c]					0.14 ± 0.01
22.9	1.7 ± 0.3	0.7 ± 0.2				0.24 ± 0.03
27.1	8.0 ± 1.6	5.1 ± 1.2	1.7 ± 0.3	0.6 ± 0.2	<0.17[d]	0.28 ± 0.01
28.2	11.0 ± 1.8	9.1 ± 2.0				0.29 ± 0.07
31.3	5.9 ± 1.5	5.1 ± 1.3				0.22 ± 0.02
35.4	1.9 ± 0.4	0.95 ± 0.02				0.18 ± 0.04

[a] Absolute intensities were determined by comparison to the 1049 cm^{-1} line of NO_3^- as described in the text. [b] The Raman depolarization ratio for the fundamental transition involving the symmetric stretch. This ratio corresponds to the scattered intensity with polarization perpendicular to that of the incident radiation divided by the scattered intensity with parallel polarization. [c] Errors represent one standard deviation from the mean. [d] Cross section represents an upper limit for scattering intensity as determined by comparison of the signal-to-noise ratio to the measured intensity of $2\nu_1$.

Spectra were obtained by interleaving individual spectra for either parallel or perpendicular scattering polarizations and integrating 2−5 min per scan depending on excitation wavelength. Five spectra were taken for both polarization settings for a total of 10−50 min integration time per polarization. The depolarization ratio of the NO_3^- transition at 1049 cm^{-1} is known (0.04); therefore, this transition was used as an internal depolarization standard in these measurements.[54,55]

Absolute Scattering Cross Sections. Determination of the resonance Raman cross-sections of OClO was performed as follows. First, the scattering intensities for both OClO and NO_3^- were determined by integration of peak areas. Given the separation between the OClO, NO_3^-, and water transitions, this method was found to produce intensities equivalent to those determined by nonlinear least-squares fitting the spectra to a sum of Gaussian peaks convolved with a Lorentzian instrument response and linear background. Given the scattering intensities, OClO and NO_3^- concentrations, and the depolarization ratios, the absolute Raman cross sections were calculated as follows:

$$\frac{\sigma_{\mathrm{OClO}}}{\sigma_{\mathrm{KNO_3}}} = \frac{I_{\mathrm{OClO}} c_{\mathrm{KNO_3}}}{I_{\mathrm{KNO_3}} c_{\mathrm{OClO}}} \frac{[(1+2\rho)/(1+\rho)]_{\mathrm{KNO_3}}}{[(1+2\rho)/(1+\rho)]_{\mathrm{OClO}}} \quad (1)$$

In the above equation, c is concentration, ρ is the depolarization ratio, I is intensity, and σ is the cross section in units of Å^2. The wavelength-dependent cross sections of NO_3^- were obtained by extrapolation of the absolute intensities reported in the literature.[54,55] The absolute resonance Raman cross sections are presented in Table 1 where the reported error represents one standard deviation from the mean of 3−10 measurements depending on excitation wavelength.

Data Analysis. Calculation of the absorption and Raman cross sections was performed using the time-dependent formalism of Lee and Heller.[50−52,60,61] In this approach, the Raman and absorption cross sections are given by

$$\sigma_{\mathrm{R}}(E_{\mathrm{l}}) = \frac{8\pi E_{\mathrm{s}}^{\,3} E_{\mathrm{l}} e^4 M_{\mathrm{eg}}^{\,4}}{9\hbar^6 c^4} \int_{-\infty}^{\infty} \partial E_{00} H(E_{00}) \left| \int_0^{\infty} \langle \mathrm{f}|\mathrm{i}(t)\rangle \times \exp[\mathrm{i}(E_{\mathrm{l}} + E_{\mathrm{i}})t/\hbar] D(t)\, \mathrm{d}t \right|^2 \quad (2)$$

$$\sigma_{\mathrm{A}}(E_{\mathrm{l}}) = \frac{4\pi e^2 E_{\mathrm{l}} M_{\mathrm{eg}}^{\,2}}{6\hbar^2 cn} \int_{-\infty}^{\infty} \partial E_{00} H(E_{00}) \int_{-\infty}^{\infty} \langle \mathrm{i}|\mathrm{i}(t)\rangle \times \exp[\mathrm{i}(E_{\mathrm{l}} + E_{\mathrm{i}})t/\hbar] D(t)\, \mathrm{d}t \quad (3)$$

where M is the transition moment of the photochemically relevant transition, E_{00} is the difference in energy between the ground and excited electronic states, E_{l} is the energy of the incident radiation, E_{s} is the energy of the scattered light, and E_{i} is the energy of the initial vibrational state. $D(t)$ is the homogeneous line width, which is composed of both pure dephasing and population decay. As in our previous study,[36] a Gaussian functional form for the homogeneous line width was found to best reproduce the red edge of the absorption spectrum (see below) and was therefore employed in this study. $H(E_{00})$ represents inhomogeneous broadening corresponding to the distribution of E_{00} energies created by different solvent environments that are static on the time scale of Raman scattering. The solvent site distribution was modeled as Gaussian with reported values for the inhomogeneous broadening representing the standard deviation of this distribution. The $\langle \mathrm{f}|\mathrm{i}(t)\rangle$ term in eq 2 represents the overlap of the final state in the scattering process with the initial state propagating under the influence of the excited-state Hamiltonian. The $\langle \mathrm{i}|\mathrm{i}(t)\rangle$ term in eq 3 is the corresponding term involving the initial ground state and the propagating state. The lowest frequency mode of OClO is at 450 cm^{-1}; therefore, the initial state is taken to be the ground vibrational state along all coordinates (i.e., the 0 K approximation is assumed to be valid).

The model employed for the optically prepared, $^2A_2$ excited-state potential energy surface was as follows:

$$V_{\mathrm{e}} = \frac{1}{2}\frac{\omega_{\mathrm{e1}}}{\omega_{\mathrm{g1}}}(q_1 - \Delta_1)^2 + \frac{1}{2}\frac{\omega_{\mathrm{e2}}}{\omega_{\mathrm{g2}}}(q_2 - \Delta_2)^2 + \frac{1}{2}\frac{\omega_{\mathrm{e3}}}{\omega_{\mathrm{g3}}}(q_3)^2 + \frac{1}{6}\chi_{111}\left(\frac{\omega_{\mathrm{e1}}}{\omega_{\mathrm{g1}}}\right)^{3/2}(q_1 - \Delta_1)^3 + \frac{1}{2}\chi_{133}\left(\frac{\omega_{\mathrm{e1}}}{\omega_{\mathrm{g1}}}\right)^{1/2}\left(\frac{\omega_{\mathrm{e3}}}{\omega_{\mathrm{g3}}}\right)(q_1 - \Delta_1)(q_3)^2 + A\exp\left(-a^2 q_3^{\,2}\frac{\omega_{\mathrm{e3}}}{\omega_{\mathrm{g3}}}\right) \quad (4)$$

where ω_{g} and ω_{e} are the ground- and excited-state frequencies along the symmetric stretch, bend, and asymmetric stretch denoted by the subscripts 1, 2, and 3, respectively. The first three terms in eq 4 represent the harmonic contributions to the potential. Displacement of the excited-state potential energy surface minimum relative to the ground state along each coordinate is denoted as Δ, with displacement incorporated only for the bend and symmetric stretch degrees of freedom since these modes are totally symmetric in the C_{2v} point group of ground-state OClO. Terms in eq 4 containing χ_{nnn} represent anharmonic contributions to the potential. Specifically, the term containing χ_{111} is the cubic anharmonicity term involving the symmetric stretch only. Anharmonic coupling between the symmetric and asymmetric stretch coordinates is represented by the χ_{133} term.

The nature of the $^2A_2$ potential surface along the asymmetric stretch is a matter of some controversy. Gas-phase absorption studies suggest that the potential along this coordinate is harmonic with $\omega_{\mathrm{e}} = 571$ cm^{-1} and a Gaussian barrier ($A =$

1673 cm^{-1} and $a^2 = 0.024$) centered at $Q_3 = 0$.[6] In contrast, ab initio calculations suggest that the potential along the asymmetric stretch is harmonic with $\omega_e = 437$ cm^{-1}.[48] Finally, the RRIA of OClO dissolved in cyclohexane demonstrated that neither of these models is capable of reproducing the intensity of the asymmetric stretch overtone transition in solution, and the intensity was found to be consistent with only a modest reduction in the excited-state frequency to ~750 cm^{-1}.[36] These models, harmonic with and without a Gaussian barrier, were explored in our analysis, and the potential barrier is incorporated into the description of the $^2A_2$ surface through the final term in eq 4.

Calculation of the time-dependent overlaps ($\langle i|i(t)\rangle$ and $\langle f|i(t)\rangle$) was performed as follows. First, when the symmetric and asymmetric stretch coordinates are anharmonically coupled, these vibronic degrees of freedom are no longer separable such that the two-dimensional vibrational time correlator must be calculated. This was accomplished using the approximate time propagator algorithm of Feit and Fleck.[62,63] In this approach, the initial state propagating under the influence of the excited-state Hamiltonian is given by

$$|i(t)\rangle = \exp(i(\Delta t)\nabla^2/4M)\exp(-i(\Delta t)V_e)\times \exp(i(\Delta t)\nabla^2/4M)|i(0)\rangle + \vartheta(\Delta t^3) \quad (5)$$

where ∇^2 is the Laplacian in position space, V_e is the excited-state potential, and Δt is the propagation time step. The total overlap was then determined by multiplying this two-dimensional overlap by the one-dimensional overlap involving the bend. The one-dimensional overlap was determined using the method of Mukamel and co-workers.[64] Two-dimensional propagations were performed on a 600 × 600 grid, and given that the error in the approximate time propagator method scales as the third power of the time step, a minimum step size of 0.5 fs was employed. Overlaps were determined for times up to ~0.5 ps, resulting in a total computational time of 4.5 h/overlap.

For calculations in which anharmonicity between coordinates was not included, the three vibronic degrees of freedom were modeled as separable, and the multidimensional overlap was reduced to the product of the one-dimensional overlaps:

$$\langle i|i(t)\rangle = \prod_{k=1}^{3}\langle i|i(t)\rangle_k \quad (6)$$

$$\langle f|i(t)\rangle = \langle f|i(t)\rangle\prod_{k=1}^{2}\langle i|i(t)\rangle_k \quad (7)$$

The expression for $\langle f|i(t)\rangle$ in eq 7 represents the case where only a single degree of freedom is Raman-active (i.e., fundamental and overtone transitions). Calculation of the multidimensional overlap then consists of determining the individual overlaps along each coordinate. A one-dimensional approximate time propagator calculation employing a time step of 0.2 fs was used to determine the overlap for the symmetric stretch since anharmonicity along this coordinate was found to be necessary in order to reproduce the vibronic progressions observed in the absorption spectrum (see below). The bend and asymmetric stretch coordinates were modeled as harmonic with frequency change between the ground and excited state, with calculation of the time-dependent overlaps for these degrees of freedom performed using the method of Mukamel and co-workers.[64]

In the above analysis, it is assumed that the resonance Raman scattering originates from the $^2A_2$ state. However, the depolarization ratios reported in Table 1 are all below 0.33, demonstrating that more than one state contributes to the observed scattering. A similar depression of the depolarization ratios below 0.33 was also observed for OClO dissolved in cyclohexane.[36] We recently reported a detailed analysis of the depolarization ratios, absolute resonance Raman cross sections, and absorption cross sections for OClO in cyclohexane in the limit where two optically active states participate in the scattering process.[35] Two conclusions concerning the validity of the single-state approximation in the analysis of the resonance Raman and absorption cross sections of OClO were made. First, the depolarization ratios were found to be consistent with the presence of the optically weak, $^2A_1$ state in energetic proximity to the $^2A_2$ surface; however, the coupling between the $^2A_2$ and $^2A_1$ states is modest such that the surfaces can be modeled as separable. Second, the smaller transition moment and larger homogeneous line width of the $^2B_1 - ^2A_1$ transition limits the scattering contribution of the $^2A_1$ state to <5% that of the $^2A_2$ state. In short, it was found that the single-state approach to modeling the resonance Raman and absorption cross sections of OClO results in an accurate description of the $^2A_2$ surface. Given the similarity of the depolarization ratios in water and cyclohexane (see below), we assume that a comparable situation exists for aqueous OClO and that the single-state approximation provides an accurate description of the $^2A_2$ surface in water.

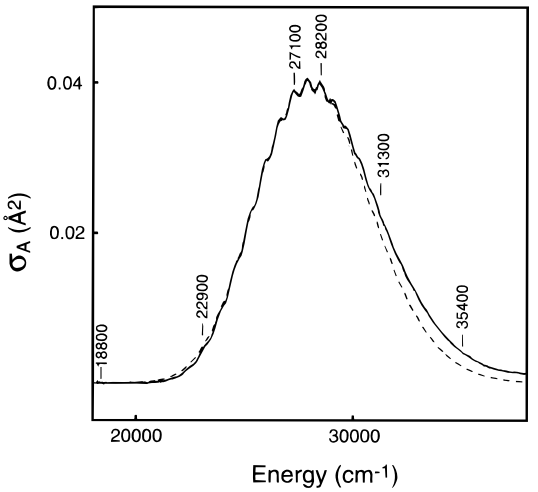

Figure 1. Experimental (solid line) and calculated (dashed line) electronic absorption spectra of aqueous chlorine dioxide in the region of the $^2B_1 - ^2A_2$ transition. Computational methods and the potential energy surface parameters employed in the calculation are given in the text. Excitation frequencies at which absolute resonance Raman cross sections were measured are indicated.

Experimental Results

Absorption Spectrum. The absorption spectrum of OClO dissolved in water is presented in Figure 1. Spectra obtained in this lab are in good agreement with previous studies where the absorption cross section was determined to be 0.040 Å^2 at 360 nm.[31,65] It should be noted that the vibronic structure observed in the absorption spectrum is much less pronounced for aqueous OClO relative to cyclohexane, demonstrating that the extent of spectral broadening increases in water. An increase in either the homogeneous or inhomogeneous line width would serve to increase the diffuseness of the absorption spectrum; therefore, the absorption spectrum alone cannot be used to differentiate between broadening mechanisms. However, analysis of the absolute resonance Raman intensities demonstrates that the increase in diffuseness is dominated by an increase in the inhomogeneous line width (see below).

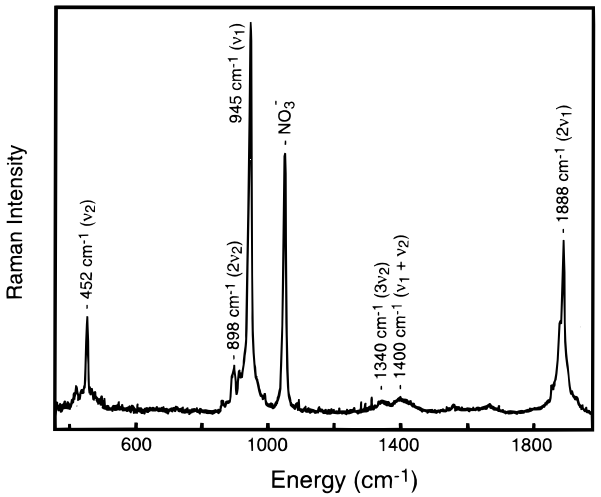

Figure 2. Resonance Raman spectrum of chlorine dioxide dissolved in water obtained with 368.9 nm excitation. The peak marked with NO_3^- corresponds to nitrate ion which was quantitatively added to provide an internal scattering standard. Intensity assignable to the symmetric stretch (ν_1) and bend (ν_2) is observed. Intensity observed at 1400 cm^{-1} contains contributions from the water/KNO_3 background.

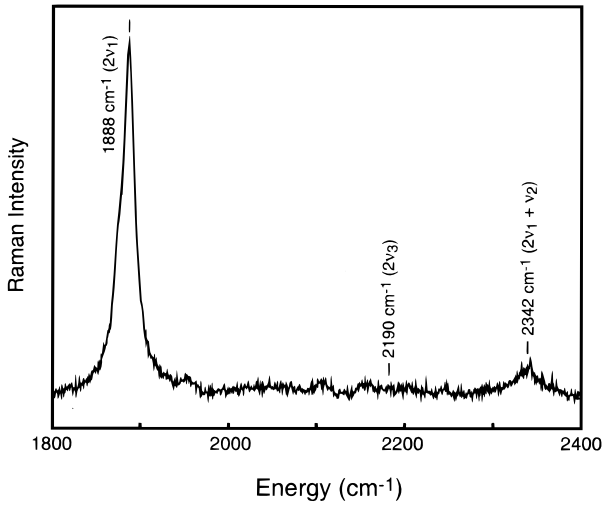

Figure 3. Overtone region of the resonance Raman spectrum of chlorine dioxide dissolved in water obtained with 368.9 nm excitation. The symmetric stretch overtone transition and a combination band are observed (ν_1 and ν_2 refer to the symmetric stretch and bend, respectively). Also denoted is the expected location for the asymmetric stretch overtone transition. No intensity assignable to this transition is observed.

Resonance Raman Intensities. The resonance Raman spectrum of OClO in aqueous solution obtained with 368.9 nm excitation is presented in Figure 2. In addition, the absolute resonance Raman cross sections determined for all excitation wavelengths utilized in this study are reported in Table 1. The contribution of each vibrational coordinate to the spectra and comparison of the intensities observed here to those previously measured for OClO dissolved in cyclohexane are presented below.

Symmetric Stretch (ν_1). The most intense features in the Raman spectra correspond to the symmetric stretch fundamental and overtone transitions at 945 and 1888 cm^{-1}, respectively (Figure 2). Transitions involving the second and third overtones of this mode are also observed (data not shown) but were not explicitly analyzed in this study. The fundamental transition is shifted to higher frequency by $\sim$7 cm^{-1} in aqueous solution relative to cyclohexane. Splitting of the transitions is observed corresponding to the presence of OClO incorporating different Cl isotopes (^{35}Cl and ^{37}Cl) with intensities in agreement with the isotopic abundance. At 368.9 nm, the absolute scattering cross sections of the fundamental and overtone transitions are 8.0×10^{-10} and 5.1×10^{-10} $Å^2$, respectively (Table 1). These values are similar to the corresponding values determined in cyclohexane (6.9×10^{-10} and 3.75×10^{-10} $Å^2$, respectively).

Bend (ν_2). The fundamental and overtone transitions of the bend are observed at 452 and 898 cm^{-1}, respectively. The Raman cross section for the fundamental transition of ν_2 in water is 1.7×10^{-10} $Å^2$ (Table 1), similar to the value determined in cyclohexane.

Asymmetric Stretch (ν_3). By symmetry, fundamental intensity corresponding to the asymmetric stretch is not expected since this coordinate is nontotally symmetric in the C_{2v} point group of ground-state OClO. No intensity is observed at 1100 cm^{-1}, confirming this expectation (Figure 2). Even overtone transitions involving nontotally symmetric coordinates can be observed if the excited-state frequency differs from that of the ground state. Figure 3 presents an expanded view of the 368.9 nm resonance Raman spectrum in the region where the overtone transition for the asymmetric stretch is expected. As the figure illustrates, no intensity assignable to the overtone transition of the asymmetric stretch is observed. This is in contrast to the observation of a transition in cyclohexane at 2190 cm^{-1}. An upper limit to the intensity of this transition can be established by comparison to the overtone transition of the symmetric stretch. Given the signal-to-noise ratio of the spectrum (about 30:1), the cross section of the asymmetric stretch overtone transition is estimated to be $\leq 1.7 \times 10^{-11}$ $Å^2$.

Computational Results

Modeling of the $^2A_2$ Potential Energy Surface. A comparison of the calculated and experimentally measured electronic absorption spectra is presented in Figure 1. The $^2A_2$ excited-state potential energy surface parameters determined from simultaneous analysis of the resonance Raman and absorption cross sections are presented in Table 2. As Figure 1 illustrates, this model is capable of reproducing the observed vibrational progressions and overall intensity of the absorption spectrum. The absorption cross sections at higher frequencies are underestimated; however, other transitions located further in the UV and/or the presence of a weak transition to the $^2A_1$ state may contribute to the absorption intensity in this region.[35,66,67] In particular, the resonance Raman depolarization ratios are less than 0.33 (Table 1), an observation that is consistent with the participation of a second excited state in the scattering process (see above).[35,56,68]

The spectral breadth evident in the absorption spectrum is more extensive in water than in cyclohexane or the gas phase, suggesting that the homogeneous and/or inhomogeneous line widths are larger in aqueous solution. Comparison of the calculated and experimentally determined absolute resonance Raman scattering cross sections provides a method by which to partition between these line widths. Figure 4 presents a comparison of the experimental and calculated Raman cross sections for both the fundamental and overtone transition of the symmetric stretch with homogeneous and inhomogeneous line widths of 85 $\pm$ 10 and 280 $\pm$ 20 cm^{-1}, respectively. In addition, the predicted cross sections when all broadening is incorporated as homogeneous (220 cm^{-1}) is presented. This comparison demonstrates that the symmetric stretch fundamental and overtone intensities are systematically underestimated when all broadening is incorporated as homogeneous; however, the

TABLE 2: $^2A_2$ Excited-State Potential Energy Surface Parameters for OClO in Water[a]

transition[b]	ω_g (cm^{-1})[c]	ω_e (cm^{-1})	Δ[d]	anharm[e] (cm^{-1})	σ_R(exp)[f] ($\times 10^{10}$ Å^2)	σ_R(calc) ($\times 10^{10}$ Å^2)
ν_1	945	685	5.63	−15	8.0	8.2
ν_2	450	284	0.4	0	1.7	2.4
ν_3	1100	850	0	0		
$2\nu_1$			5.63		5.1	7.3
$2\nu_2$			0.4		0.6	0.4
$2\nu_3$			0		<0.17	0.17

[a] Calculation performed with a Gaussian homogeneous line width. Best fit to the experimental cross sections resulted in $\Gamma = 85 \pm 15$ cm^{-1}, inhomogeneous standard deviation $= 280 \pm 20$ cm^{-1}, $M_{eg} = 0.363$ Å, $E_{oo} = 18\,900$ cm^{-1}, $n = 1.35$. [b] Raman transition for which the calculation is performed. The symbols ν_1, ν_2, and ν_3 refer to the symmetric stretch, bend, and asymmetric stretch, respectively. The first three terms correspond to fundamental transitions, and the next three terms refer to overtone transitions. [c] ω_g refers to the ground-state harmonic frequency, and ω_e is the excited-state harmonic frequency. [d] Dimensionless displacement of the excited-state potential energy surface minimum relative to the ground state. [e] Anharmonicity prefactor for the cubic term in the series expansion of the potential energy surface. By comparison to the description of the Morse oscillator, this term is equal to $(w_e/2)^{1.5}/D_e^{0.5}$ in dimensionless units where w_e is the excited-state harmonic frequency and D_e is the Morse dissociation energy given by $w_e^2/(4w_ex_e)$ where x_e is the anharmonicity parameter.[84] [f] Experimental Raman cross sections corresponding to 368.9 nm excitation as reported in Table 1.

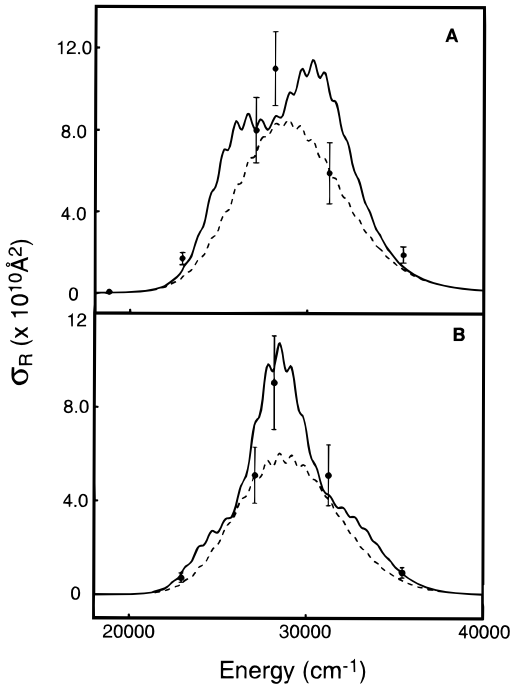

Figure 4. Experimental and calculated absolute resonance Raman cross sections for the symmetric stretch fundamental (A) and overtone (B) transitions. Calculations were performed employing homogeneous broadening of 85 ± 15 cm^{-1} and inhomogeneous broadening of 280 ± 20 cm^{-1} (solid line), as well as homogeneous broadening of 220 cm^{-1} and no inhomogeneous broadening (dashed line).

predicted intensities are not dramatically reduced by an increase in the homogeneous line width.

The absolute resonance Raman cross sections of the symmetric stretch fundamental and overtone transitions provide limited constraint on the homogeneous line width; however, the fundamental transition of the bend is extremely sensitive to homogeneous broadening. The calculated intensity of this transition decreases by almost 2 orders of magnitude with an increase in homogeneous line width from 85 to 220 cm^{-1}. This

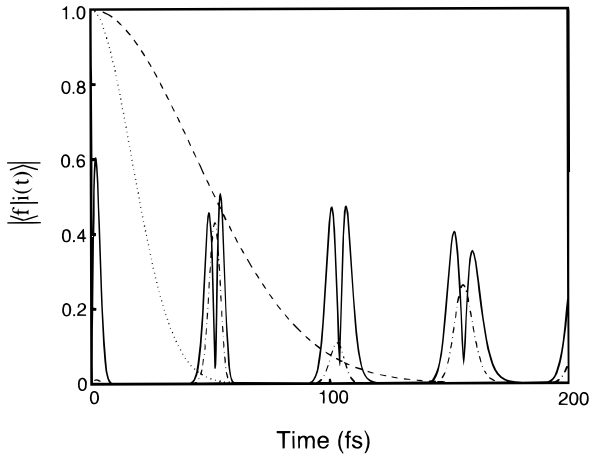

Figure 5. Multidimensional Raman time correlators ($|\langle f|i(t)\rangle|$) for the fundamental transitions of the symmetric stretch (solid line) and bend (dash−dot line). Also presented is the decay introduced by homogeneous broadening for line widths of 85 cm^{-1} (dashed line) and 220 cm^{-1} (dotted line). The figure demonstrates that the time correlator for the symmetric stretch fundamental transition develops the majority of its intensity in the first 10 fs. Given this rapid buildup and decay, the predicted intensity for this transition is not dramatically affected by an increase in the homogeneous line width. However, the slower dynamics for the bend time-correlator result in the intensity of this transition being substantially reduced by an increase in homogeneous broadening.

behavior can be understood within the time-dependent formalism of Raman scattering. Figure 5 presents the multidimensional $\langle f|i(t)\rangle$ (i.e., eq 7) for the fundamental transitions involving the symmetric stretch (solid line) and bend (dashed−dotted line). In addition, decays corresponding to homogeneous line widths of 85 (dashed line) and 220 cm^{-1} (dotted line) are also presented. At early times (0−10 fs), the amplitude of the time correlators is determined by evolution along the symmetric stretch coordinate. The dynamics along this coordinate are more rapid than the decay due to homogeneous broadening such that the predicted intensity of the symmetric stretch fundamental transition is affected only to a limited extent by homogeneous broadening. In contrast, the time correlator for the bend acquires the majority of its intensity at ∼50 fs. An increase in the homogeneous line width from 85 to 220 cm^{-1} results in the truncation of the time correlator before 50 fs such that the predicted intensity of the bend fundamental transition is dramatically reduced. Therefore, simultaneous reproduction of absolute scattering cross sections for the symmetric stretch fundamental and overtone transitions as well as the bend fundamental transition constrains the homogeneous line width to 85 ± 15 cm^{-1}. Given this line width, reproduction of the spectral breadth observed in the absorption spectrum requires an additional amount of inhomogeneous broadening corresponding to a standard deviation of 280 ± 20 cm^{-1}.

Figure 3 demonstrates that intensity is not observed for the overtone transition of the asymmetric stretch. Estimation of the signal-to-noise ratio combined with the intensity of the symmetric stretch overtone transition provides an upper limit for the Raman cross section of this transition of 1.7×10^{-11} Å^2. Figure 6 demonstrates that this intensity is consistent with a decrease in the excited-state frequency to 850 ± 25 cm^{-1} employing a harmonic model for the excited-state potential energy surface along this coordinate (solid line). Further reduction in the excited-state frequency results in predicted intensities that are greater than the intensity limit. Figure 6 presents the overtone intensity predicted using the gas-phase (dotted line) and ab initio (dotted−dashed line) potentials along this coordinate. Both the gas-phase and ab initio potential

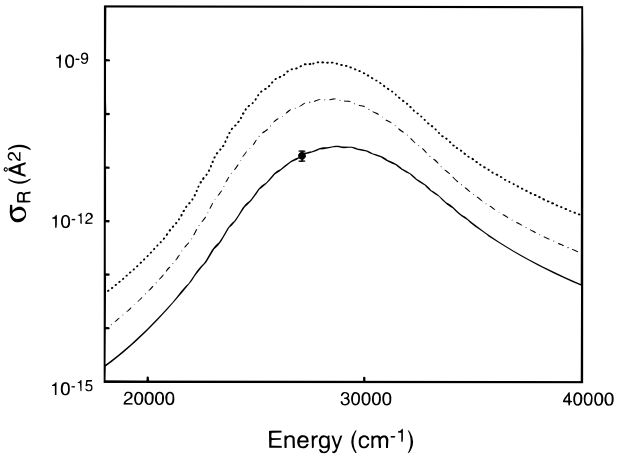

Figure 6. Experimental limit for intensity of the asymmetric stretch overtone transition (point). Also depicted are the calculated resonance Raman excitation profiles of this transition employing a harmonic description of the asymmetric stretch coordinate with excited-state frequency 850 cm^{-1} (solid line), the ab initio potential (dash−dot), and gas-phase potential (dotted). The figure demonstrates that the ab initio and gas-phase potentials significantly overestimate the intensity of this transition.

energy surfaces were found to be inconsistent with the absence of intensity for the asymmetric stretch overtone transition in that these potentials result in predicted intensities that are significantly larger than the intensity limit. It is important to note that partitioning of the homogeneous and inhomogeneous line widths through absolute resonance Raman intensities is necessary in order to perform the above analysis. If the homogeneous line width were ambiguous, the cross sections predicted by the ab initio or gas-phase models could potentially be reduced by simply increasing the homogeneous line width. However, the acquisition and quantitative analysis of absolute resonance Raman cross sections performed in this study removes any ambiguity in the amount of homogeneous broadening to employ.

Effect of Intercoordinate Anharmonicity. Investigations on the influence of anharmonic coupling on the predicted intensity for the asymmetric stretch overtone transition were performed by including coupling between the symmetric and asymmetric stretch coordinates through the term containing χ_{133} in eq 4. Values of χ_{133} as large as ~150 were investigated consistent with previous estimates.[69] Even with the inclusion of anharmonic coupling, the predicted intensity for the asymmetric stretch overtone transition employing the ab initio or gas-phase potentials is still significantly larger than the experimental intensity limit. Therefore, anharmonic coupling between the symmetric and asymmetric stretch coordinates does not significantly alter the results and conclusions presented here.

The Excited-State Equilibrium Structure of Aqueous OClO. The parameters for the $^2A_2$ surface determined in our analysis (Table 2) can be used to define the equilibrium excited-state geometry provided that the relationship between dimensionless normal coordinates and internal coordinates is known. The ab initio theoretical results of Peterson and Werner can be used to establish this relationship.[48,49] In these calculations, the ground-state potential was defined in terms of the following symmetry coordinates:

$$S_1 = \frac{r_1 + r_2}{\sqrt{2}} \qquad S_2 = \theta \qquad S_3 = \frac{r_1 - r_2}{\sqrt{2}} \tag{8}$$

where the S_n are the symmetry coordinates related to the symmetric stretch, bend, and asymmetric stretch ($n = 1$, 2, and 3, respectively), and these are given as linear combinations of the internal coordinates corresponding to ClO bond lengths (r_n) and the O−Cl−O bond angle (Θ). The relationship between normal and symmetry coordinates can be determined by Wilson-FG matrix analysis of the ab initio ground-state potential energy surface. This analysis results in the following transformation between symmetry and normal coordinates:

$$\begin{bmatrix} S_1 \\ S_2 \\ S_3 \end{bmatrix} = \begin{bmatrix} 0.098 & -0.013 & 0 \\ -0.021 & -0.079 & 0 \\ 0 & 0 & -0.106 \end{bmatrix} \begin{bmatrix} Q_1 \\ Q_2 \\ Q_3 \end{bmatrix} \tag{9}$$

where the coefficients in the conversion matrix are given in atomic units, and coefficients smaller than 0.001 are ignored. The above calculation was performed with positive displacement defined as an increase in bond length and O−Cl−O bond angle. Using the above relationship, the dimensionless displacements of the $^2A_2$ excited state determined by RRIA can be used to define the geometry changes that occur on this surface. The equilibrium geometry of ground-state OClO corresponds to ClO bond lengths of 1.471 Å and O−Cl−O bond angle of 117.35°.[70] The displacements along the symmetric stretch ($\Delta = 5.63$) and bend ($\Delta = 0.4$) in water correspond to a $^2A_2$ excited-state equilibrium geometry with Cl−O bond lengths of 1.68 Å and O−Cl−O bond angle of 108.8°. Since resonance Raman intensities depend on Δ^2, the calculation is performed such that the sign of Δ along the symmetric stretch or bend corresponds to Cl−O bond elongation and reduction of the O−Cl−O bond angle in agreement with both gas-phase experimental and theoretical results.[1]

Discussion

Excited-State Structural Relaxation and Photoproduct Formation. The analysis presented above provides a mode-specific description of the excited-state structural relaxation of aqueous OClO that occurs following photoexcitation. The relaxation is dominated by evolution along the symmetric stretch and bend coordinates, with limited evolution occurring along the asymmetric stretch. These dynamics are similar to those determined in our previous study of OClO dissolved in cyclohexane.[36] For both solvents, the lack of excited-state structural evolution along the asymmetric stretch results in the preservation of C_{2v} symmetry on the $^2A_2$ surface. These dynamics stand in contrast to the evolution observed in the gas phase where excited-state structural relaxation along the asymmetric stretch coordinate results in the reduction of molecular symmetry to C_s.[6,7]

The preservation of C_{2v} symmetry on the $^2A_2$ surface for aqueous OClO is potentially responsible for the increase in the Cl formation quantum yield (Φ_{Cl}) in water relative to the gas phase. Previous gas-phase experimental and theoretical studies have suggested that a geometry at or near C_{2v} symmetry is necessary for Cl formation. Recent calculations by Peterson and Werner have indicated that the reduction of symmetry from C_{2v} to C_s serves to reduce the energy barrier for ClO and O formation.[48,49] Furthermore, only for geometries at or near C_{2v} symmetry was the production of Cl and O_2 predicted to be energetically favorable. This conclusion is consistent with recent studies of Davis and Lee on the translational energy distribution of products formed from photolysis of gas-phase OClO where the production of O_2 was suggested to occur through a C_{2v} transition state.[14] These researchers also found that excitation of the asymmetric stretch coordinate results in

roughly a 10-fold reduction in Φ_{Cl}. The results presented here combined with our previous study in cyclohexane suggest that a similar mechanism for photoproduct formation is operative in these solvents. The weak intensity for the asymmetric stretch overtone transition in both water and cyclohexane demonstrates that limited excited-state evolution occurs along this coordinate. The reduction in asymmetric structural evolution on the $^2A_2$ surface results in the preservation of C_{2v} symmetry, thereby enhancing Φ_{Cl}.

The similarity in excited-state structural evolution for OClO dissolved in water and cyclohexane combined with studies of O_2 production following OClO photoexcitation demonstrates that, in addition to the $^2A_2$ surface, the lower energy $^2A_1$ and $^2B_2$ states also participate in photoproduct formation. The sequence of events in OClO photochemistry is believed to be as follows: photoexcitation to the $^2A_2$ surface results in production of the $^2A_1$ state via internal conversion through spin−orbit coupling. Production of the lower energy $^2B_2$ state then occurs by internal conversion from the $^2A_1$ surface. Studies of O_2 emission following photoexcitation of OClO in polar and nonpolar solvents have demonstrated that in D_2O the production of atomic chlorine is dominated by the Cl + $O_2(^3\Sigma_g^-)$ channel; however, in C_6D_6 and CCl_4 the Cl + $O_2(^1\Delta_g)$ channel dominates.[29] Under C_{2v} symmetry, only the $^2B_2$ state correlates with the Cl + $O_2(^1\Delta_g)$ channel; therefore, the O_2 emission studies suggest that in nonpolar and polar solvents Cl is derived from the $^2B_2$ and $^2A_1$ surfaces, respectively.[1,28,71] Given the similarity of the $^2A_2$ surface parameters in water and cyclohexane, the resonance Raman results in combination with the O_2 emission results demonstrate that partitioning between the Cl + O_2 channels must occur after decay of the $^2A_2$ surface. The above discussion assumes that C_{2v} symmetry is preserved along the reaction coordinate. A reduction in molecular symmetry on the $^2A_1$ or $^2B_2$ surface would serve to substantially alter this picture. For example, symmetry reduction could result in the production of the peroxy isomer, ClOO, which is expected to undergo facile decay into Cl and $O_2(^3\Sigma_g^-)$.[72]

Excited-State Energetics and Solvent Dependence. In the above analysis, the homogeneous line width was found to be 85 ± 15 cm^{-1}. This is essentially identical to the 80 ± 10 cm^{-1} line width determined previously in cyclohexane.[36] Attempts to observe fluorescence from aqueous OClO were unsuccessful, suggesting that the homogeneous line width is dominated by excited-state population relaxation, with the magnitude of the line width placing the time scale for excited-state decay at ~60 fs. The similarity in homogeneous line width between water and cyclohexane demonstrates that the depopulation rate of the $^2A_2$ state is not sensitive to solvent. One plausible mechanism for the phase-dependent reactivity of OClO would be that the $^2A_2$, $^2A_1$, and $^2B_2$ excited states are stabilized to different extents in polar versus nonpolar solvents due to differences in charge distribution. Differential stabilization could modulate the potential energy surface interactions, thereby affecting photoproduct formation. However, preferential stabilization of the $^2A_1$ state relative to the $^2A_2$ state would be expected to modulate the depopulation rate of the $^2A_2$ surface, and the spectroscopic manifestation of this modulation should be solvent dependence of the homogeneous line width. The similarity of the homogeneous line width in water and cyclohexane suggests that differential stabilization of the excited states and/or solvent-dependent potential energy surface coupling is not responsible for the phase-dependent reactivity of OClO.

Resonance Raman depolarization ratios provide a second method by which to monitor solvent dependence of the $^2A_2$ and $^2A_1$ state excitation energies. The depolarization ratio is defined as the intensity of scattered light with polarization perpendicular to the incident field divided by the intensity of scattered light with polarization that is parallel to the incident field.[56−59] This ratio can be used to establish the presence of excited states with electronic transition moments orthogonal to the transition of interest.[56,68] For OClO, the $^2B_1$−$^2A_1$ transition moment is predicted to be orthogonal to that of the stronger $^2B_1$−$^2A_2$ transition.[1,6,7] A detailed description of resonance Raman depolarization theory is beyond the scope of this paper; however, we have recently reported a detailed analysis of these ratios for OClO dissolved in cyclohexane.[35] In this work, deviation of the depolarization ratio of the symmetric stretch fundamental transition from 0.33 (the value expected if only a single state participates in the scattering process) was observed and found to be consistent with the presence of the optically weak $^2A_1$ potential energy surface in energetic proximity to the $^2A_2$ state. If the $^2A_1$ and $^2A_2$ surfaces are stabilized to different extents, it should be reflected by a change in depolarization ratios. Figure 7 demonstrates that a subtle change in the depolarization ratios is observed in water relative to cyclohexane in that the depolarization ratios are systematically larger in water. Preliminary analysis of these data suggests that this difference is consistent with a slight increase in the excitation energy of the $^2A_1$ state in water; however, the depolarization dispersion and magnitude of the depolarization ratios are similar in both solvents, suggesting that a dramatic change in the relative energies of the $^2A_2$ and $^2A_1$ states has not occurred.

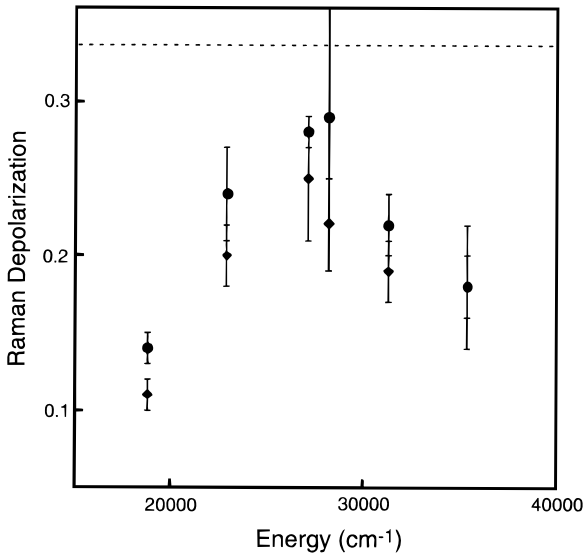

Figure 7. Resonance Raman depolarization ratio of the symmetric stretch fundamental transition in aqueous solution (circles). Also presented are the depolarization ratios for this same transition in cyclohexane (diamonds). The dashed line corresponds to a depolarization ratio of 1/3, the value predicted when a single state contributes to the scattering process. The systematic deviation of the depolarization ratios from this value is consistent with the presence of the $^2A_1$ surface in energetic proximity to the optically bright, $^2A_2$ surface.

Interaction between OClO and Water. The question remains as to the nature of the interactions between OClO and water responsible for modifying the $^2A_2$ potential energy surface. We can address this question by comparing OClO to similar compounds for which this question has been investigated. OClO is isoelectronic with O_3^-, the main difference being that OClO is a neutral radical and O_3^- is charged. The resonance Raman spectrum of aqueous O_3^- has been reported by Su and Tripathi, and the most intriguing result of this work is the ~15 cm^{-1}

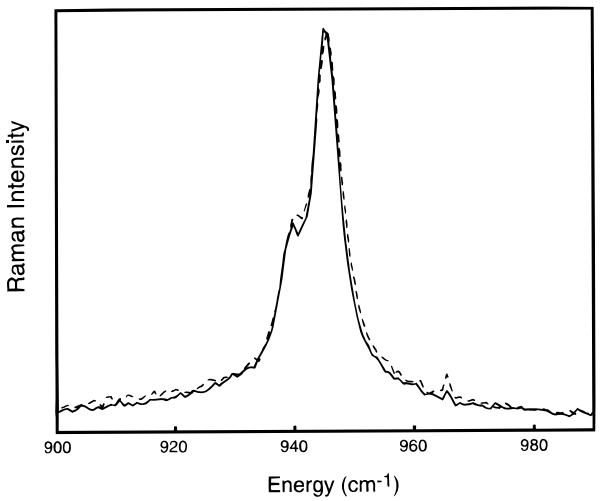

Figure 8. Resonance Raman spectra of chlorine dioxide dissolved in H_2O (dashed line) and D_2O (solid line) obtained with 368.9 nm excitation. The spectral region corresponding to the symmetric stretch fundamental transition is presented. The figure demonstrates that only a modest decrease in the line width of this transition is observed when OClO is dissolved in D_2O.

decrease in line width for the symmetric stretch fundamental transition in D_2O relative to H_2O.[73] This reduction in line width was attributed to the transition representing a combination band involving the symmetric stretch of O_3^- and solvent modes where deuteration of the solvent results in modification of the solvent-mode vibrational frequencies, thereby decreasing the apparent line width. It was suggested that the presence of charge results in strong coupling between solvent and solute vibronic degrees of freedom such that the molecular species in solution is more appropriately thought of as $(O_3(H_2O)_n)^-$. To see whether a similar spectroscopic manifestation of strong solvent−solute coupling exists for OClO, we measured the resonance Raman spectrum at 368.9 nm in both H_2O and D_2O. The comparison of the symmetric stretch region of the spectrum for these two solvents is presented in Figure 8. A decrease in line width is observed in D_2O; however, this decrease is very modest ($\sim$1 cm^{-1}), suggesting that the intermolecular coordinate for aqueous OClO is much weaker than for aqueous O_3^-.

A second measure of solute−solvent interaction is provided by the rotational correlation time of OClO. Studies on the rotational dynamics of small molecular ions in polar−protic and −aprotic solvents have demonstrated that an increase in solute−solvent coupling strength is manifested as an increase in the rotational correlation time.[74−77] The rotational correlation time of aqueous OClO is 0.6 ps, in agreement with the predicted time employing a hydrodynamic slip model, suggesting that the solvent−solute interactions between OClO and water are weak.[33] Furthermore, the rotational correlation time of OClO is markedly shorter than the corresponding 2.3 ps time for aqueous O_3^- supporting the existence of stronger solvent−solute interactions for aqueous O_3^-.[78] Rotational correlation times greater that those predicted by a stick boundary condition have been observed for molecular ions (NO_3^-, NCS^-, NCO^-) dissolved in polar−protic solvents, consistent with the existence of solvent−solute hydrogen bonding.[74] The rotational correlation times for OClO and O_3^- are significantly shorter than those predicted by a stick boundary condition, suggesting that hydrogen bonding is not the dominant interaction for either species in solution. A formal test of this hypothesis would be to measure the rotational correlation time of OClO in a series of polar−protic and −aprotic solvents to ascertain whether rotational dynamics are indeed affected by the presence of hydrogen bonding and/or electrostatic interaction with the solvent.

Given that the interaction between OClO and water is weaker than for aqueous O_3^- and that intermolecular hydrogen bonding is not the largest component of the solvent coordinate, we are left to conclude that dipole−dipole interactions dominate the solvent response to OClO photoexcitation. For OClO in cyclohexane, we suggested that dipole−induced dipole forces were responsible for altering the $^2A_2$ excited-state potential energy surface along the asymmetric stretch coordinate. The change in dipole moment with respect to normal coordinate displacement is largest for the asymmetric stretch; therefore, a mechanism was proposed where solvent reorientation in response to motion along the asymmetric stretch coordinate restricts evolution along this coordinate. Given the absence of intensity of the overtone transition of the asymmetric stretch in water, we conclude that a similar mechanism is operative in aqueous OClO. It should be noted that studies on the solvation dynamics of water have demonstrated that the majority of the dynamics occur on the $<$50 fs time scale.[79−81] However, the large increase in inhomogeneous line width in water relative to cyclohexane suggests that for OClO the relevant component of the solvent response is operative on times slower than the time scale for Raman scattering. Therefore, slower relaxing solvent degrees of freedom such as diffusional dielectric relaxation and intermolecular hydrogen bonding probably make the largest contribution to the solvent coordinate.

A second, similar mechanism for the solvent-dependent photochemistry of OClO was proposed based on a study of product yields in CCl_4.[82] In this study, enhancement of the Cl + O_2 channel was believed to occur via symmetry breaking of the excited state due to dipole−induced dipole solvent−solute interactions. In an elegant study by Johnson and Myers, dynamical symmetry reduction of the excited-state geometry due to solvation was observed for I_3^-.[83] The spectroscopic manifestation of this symmetry reduction was the appearance of resonance Raman intensity corresponding to the fundamental transition of the asymmetric stretch, a transition that is nominally forbidden by symmetry. The RRIA studies of OClO dissolved in water and cyclohexane demonstrate that no intensity assignable to the fundamental of the asymmetric stretch is observed consistent with the preservation of C_{2v} symmetry on the $^2A_2$ surface. However, the existence of dynamical symmetry breaking in CCl_4 has yet to be explored by resonance Raman spectroscopy.

Conclusions

In this paper, we have reported the analysis of the absolute resonance Raman and absorption cross sections of aqueous OClO. It was demonstrated that, similar to the dynamics in cyclohexane, excited-state evolution along the asymmetric stretch coordinate is restricted relative to the dynamics that occur in the gas phase. The absence of significant evolution along this coordinate results in the preservation of C_{2v} symmetry on the $^2A_2$ surface. This preservation of symmetry potentially results in an increase in the Cl photochemical quantum yield in aqueous solution relative to the gas phase. The homogeneous line width determined for aqueous OClO was found to be almost identical to that observed in cyclohexane; however, the inhomogeneous line width undergoes a substantial increase in water. It was proposed that solvent−solute dipolar interactions and potentially intermolecular hydrogen bonding are important components of the solvent response to OClO photoexcitation.

Investigations are currently underway to ascertain the role of intermolecular hydrogen bonding in defining the phase-dependent reactivity of OClO.

Acknowledgment. The authors would like to thank Todd Stedl for his assistance with the normal-mode analysis. The National Science Foundation is acknowledged for their support of this work through the CAREER program (CHE-9701717). Acknowledgment is also made to the donors of the Petroleum Research Fund, administered by the American Chemical Society. P.J.R. is a recipient of a Camille and Henry Dreyfus New Faculty Award.

References and Notes

(1) Vaida, V.; Simon, J. D. *Science* **1995**, *268*, 1443.
(2) Rowland, F. S. *Annu. Rev. Phys. Chem.* **1991**, *42*, 731.
(3) Burkholder, J. B.; Talukdar, R. K.; Ravishankara, A. R. *Geophys. Res. Lett.* **1994**, *21*, 585.
(4) Solomon, S.; Sanders, R. W.; Miller Jr., H. L. *J. Geophys. Res.* **1990**, *95*, 13807.
(5) Sessler, J.; Chipperfield, M. P.; Pyle, J. A.; Toumi, R. *Geophys. Res. Lett.* **1995**, *22*, 687.
(6) Richard, E. C.; Vaida, V. *J. Chem. Phys.* **1991**, *94*, 153.
(7) Richard, E. C.; Vaida, V. *J. Chem. Phys.* **1991**, *94*, 163.
(8) Vaida, V.; Solomon, S.; Richard, E. C.; Ruhl, E.; Jefferson, A. *Nature* **1989**, *342*, 405.
(9) Bishenden, E.; Donaldson, D. J. *J. Chem. Phys.* **1994**, *101*, 9565.
(10) Bishenden, E.; Donaldson, D. J. *J. Chem. Phys.* **1993**, *99*, 3129.
(11) Bishenden, E.; Haddock, J.; Donaldson, D. J. *J. Phys. Chem.* **1991**, *95*, 2113.
(12) Delmdahl, R. F.; Baumgartel, S.; Gericke, K.-H. *J. Chem. Phys.* **1996**, *194*, 2883.
(13) Baumert, T.; Herek, J. L.; Zewail, A. H. *J. Chem. Phys.* **1993**, *99*, 4430.
(14) Davis, H. F.; Lee, Y. T. *J. Chem. Phys.* **1996**, *105*, 8142.
(15) Davis, H. F.; Lee, Y. T. *J. Phys. Chem.* **1992**, *96*, 5681.
(16) Lawrence, W. G.; Clemitshaw, K. C.; Apkarian, V. A. *J. Geophys. Res.* **1990**, *95*, 18591.
(17) Tanaka, K.; Tanaka, T. *J. Mol. Spectrosc.* **1983**, *98*, 425.
(18) Flesch, R.; Wassermann, B.; Rothmund, B.; Ruhl, E. *J. Phys. Chem.* **1994**, *98*, 6263.
(19) Ruhl, E.; Jefferson, A.; Vaida, V. *J. Phys. Chem.* **1990**, *94*, 2990.
(20) Hamada, Y.; Meyer, A. J.; Michielsen, S.; Rice, S. A. *J. Mol. Spectrosc.* **1981**, *86*, 49.
(21) Michielsen, S.; Meyer, A. J.; Rice, S. A.; Novak, F. A.; Freed, K. F.; Hamada, Y. *J. Chem. Phys.* **1981**, *74*, 3089.
(22) McDonald, P. A.; Innes, K. K. *Chem. Phys. Lett.* **1978**, *59*, 562.
(23) Brand, J. C. D.; Redding, R. W.; Richardson, A. W. *J. Mol. Spectrosc.* **1970**, *34*, 399.
(24) Coon, J. B. *J. Chem. Phys.* **1946**, *14*, 665.
(25) Coon, J. B. *Phys. Rev.* **1940**, *58*, 926.
(26) Chang, Y. J.; Simon, J. D. *J. Phys. Chem.* **1996**, *100*, 6406.
(27) Dunn, R. C.; Flanders, B. N.; Simon, J. D. *J. Phys. Chem.* **1995**, *99*, 7360.
(28) Vaida, V.; Goudjil, K.; Simon, J. D.; Flanders, B. N. *J. Mol. Liq.* **1994**, *61*, 133.
(29) Dunn, R. C.; Anderson, J. L.; Foote, C. S.; Simon, J. D. *J. Am. Chem. Soc.* **1993**, *115*, 5307.
(30) Dunn, R. C.; Simon, J. D. *J. Am. Chem. Soc.* **1992**, *114*, 4856.
(31) Dunn, R. C.; Flanders, B. N.; Vaida, V.; Simon, J. D. *Spectrochim. Acta* **1992**, *48A*, 1293.
(32) Dunn, R. C.; Richard, E. C.; Vaida, V.; Simon, J. D. *J. Phys. Chem.* **1991**, *95*, 6060.
(33) Thøgersen, J.; Jepsen, P. U.; Thomsen, C. L.; Poulsen, J. A.; Byberg, J. R.; Keiding, S. R. *J. Phys. Chem. A* **1997**, *101*, 3317.
(34) Philpott, M. J.; Charalambous, S.; Reid, P. J. *Chem. Phys. Lett.* **1997**, *281*, 1.
(35) Reid, P. J.; Esposito, A. P.; Foster, C. E.; Beckman, R. A. *J. Chem. Phys.* **1997**, *107*, 8262.
(36) Esposito, A.; Foster, C.; Beckman, R.; Reid, P. J. *J. Phys. Chem. A* **1997**, *101*, 5309.
(37) Graham, J. D.; Roberts, J. T.; Anderson, L. D.; Grassian, V. H. *J. Phys. Chem.* **1996**, *100*, 19551.
(38) Graham, J. D.; Roberts, J. T.; Brown, L. A.; Vaida, V. *J. Phys. Chem.* **1996**, *100*, 3115.
(39) Brown, L. A.; Vaida, V.; Hanson, D. R.; Graham, J. D.; Roberts, J. T. *J. Phys. Chem.* **1996**, *100*, 3121.
(40) Lanzendorf, E. J.; Kummel, A. C. *Geophys. Res. Lett.* **1996**, *23*, 1521.
(41) Pursell, C. J.; Conyers, J.; Alapat, P.; Parveen, R. *J. Phys. Chem.* **1995**, *99*, 10433.
(42) Mueller, H. S. P.; Willner, H. *J. Phys. Chem.* **1993**, *97*, 10589.
(43) Johnsson, K.; Engdahl, A.; Ouis, P.; Nelander, B. *J. Mol. Struct.* **1993**, *293*, 137.
(44) Adrian, F. J.; Bohandy, J.; Kim, B. F. *J. Chem. Phys.* **1986**, *85*, 2692.
(45) Arkell, A.; Schwager, I. *J. Am. Chem. Soc.* **1967**, *89*, 5999.
(46) Rochkind, M. M.; Pimentel, G. C. *J. Chem. Phys.* **1967**, *46*, 4481.
(47) Gole, J. L. *J. Phys. Chem.* **1980**, *84*, 1333.
(48) Peterson, K. A.; Werner, H.-J. *J. Chem. Phys.* **1992**, *96*, 8948.
(49) Peterson, K. A.; Werner, H. J. *J. Chem. Phys.* **1996**, *105*, 9823.
(50) Myers, A. B. *J. Raman Spectrosc.* **1997**, *28*, 389.
(51) Myers, A. B. *J. Opt. Soc. Am. B* **1990**, *7*, 1665.
(52) Myers, A. B.; Mathies, R. A. Resonance Raman Intensities: A Probe of Excited State Structure and Dynamics. In *Biological Applications of Raman Spectrometry*; Spiro, T. G., Ed.; John Wiley & Sons: New York, 1987; Vol. 2, pp 1−58.
(53) Brauer, G. *Handbook of Inorganic Chemistry*; Academic Press: New York, 1963; Vol. 1.
(54) Loppnow, G. R.; Mathies, R. A. *Biophys. J.* **1988**, *54*, 35.
(55) Dudik, J. M.; Johnson, C. R.; Asher, S. A. *J. Chem. Phys.* **1985**, *82*, 1732.
(56) Mortensen, O. S.; Hassing, S. Polarization and Interference Phenomena in Resonance Raman Scattering. In *Advances in Infrared and Raman Spectroscopy*; Clark, R. J. H., Hester, R. E., Eds.; Heyden: London, 1980; Vol. 6, p 1.
(57) Ziegler, L. D. *J. Chem. Phys.* **1986**, *84*, 6013.
(58) Ziegler, L. D.; Chung, Y. C.; Wang, C. P.; Zhang, Y. P. *J. Chem. Phys.* **1989**, *90*, 4125.
(59) Strommen, D. P. *J. Chem. Educ.* **1992**, *69*, 803.
(60) Lee, S.-Y.; Heller, E. J. *J. Chem. Phys.* **1979**, *71*, 4777.
(61) Tannor, D. J.; Heller, E. J. *J. Chem. Phys.* **1982**, *77*, 202.
(62) Feit, M. D.; Fleck, J. A. *J. Chem. Phys.* **1983**, *78*, 301.
(63) Feit, M. D.; Fleck, J. A.; Steiger, A. *J. Comput. Phys.* **1982**, *47*, 412.
(64) Sue, J.; Yan, Y. J.; Mukamel, S. *J. Chem. Phys.* **1986**, *85*, 462.
(65) Stitt, F.; Friedlander, S.; Lewis, H. J.; Young, F. E. *Anal. Chem.* **1954**, *26*, 1478.
(66) Hubinger, S.; Nee, J. B. *Chem. Phys.* **1994**, *181*, 247.
(67) Davies, J. A.; Mason, N. J.; Marston, G.; Wayne, R. P. *J. Phys. B* **1995**, *28*, 4179.
(68) Shang, Q.-Y.; Hudson, B. S. *Chem. Phys. Lett.* **1991**, *183*, 63.
(69) Hoy, A. R.; Brand, J. C. D. *Mol. Phys.* **1978**, *36*, 1409.
(70) Krishna Pillai, M. G.; Curl, R. F. *J. Chem. Phys.* **1962**, *37*, 2921.
(71) Shuler, K. E. *J. Chem. Phys.* **1953**, *21*, 624.
(72) Jafri, J. A.; Lengsfield III, B. H.; Phillips, D. H. *J. Chem. Phys.* **1985**, *83*, 1693.
(73) Su, Y.; Tripathi, G. N. R. *Chem. Phys. Lett.* **1992**, *188*, 388.
(74) Li, M.; Owrutsky, J.; Sarisky, M.; Culver, J. P.; Yodh, A.; Hochstrasser, R. M. *J. Chem. Phys.* **1993**, *98*, 5499.
(75) Owrutsky, J. C.; Kim, Y. R.; Li, M.; Sarisky, M. J.; Hochstrasser, R. M. *Chem. Phys. Lett.* **1991**, *184*, 368.
(76) Banin, U.; Kosloff, R.; Rhuman, S. *Isr. J. Chem.* **1993**, *33*, 141.
(77) Banin, U.; Rhuman, S. *J. Chem. Phys.* **1993**, *98*, 4391.
(78) Walhout, P. K.; Silva, C.; Barbara, P. F. *J. Phys. Chem.* **1996**, *100*, 5188.
(79) Maroncelli, M. *J. Mol. Liq.* **1993**, *57*, 1.
(80) Jimenez, R.; Fleming, G. R.; Kumar, P. V.; Maroncelli, M. *Nature* **1994**, *369*, 471.
(81) Jarzeba, W.; Walker, G. C.; Johnson, A. E.; Kahlow, M. A.; Barbara, P. F. *J. Phys. Chem.* **1988**, *92*, 7039.
(82) Bursa, M. A.; Perissinotti, L. J.; Churio, M. S.; Colussi, A. J. *J. Photochem. Photobiol. A* **1996**, *101*, 105.
(83) Johnson, A. E.; Myers, A. B. *J. Chem. Phys.* **1995**, *102*, 3519.
(84) Karplus, M.; Porter, R. N. *Atoms and Molecules*; W. A. Benjamin: New York, 1970.